2020 Joint International EUROSOI Workshop and International Conference on Ultimate Integration on Silicon (EUROSOI-ULIS) | 978-1-7281-8765-5/20/$31.00 ©2020 IEEE | DOI: 10.1109/EUROSOI-ULIS49407.2020.9365283

Reduced Current Spin-Orbit Torque Switching of a Perpendicularly Magnetized Free Layer

Roberto Lacerda de Orio
Institute for Microelectronics
TU Wien
Vienna, Austria
orio@iue.tuwien.ac.at

Johannes Ender
CDL for Nonvolatile Memory and Logic
Institute for Microelectronics, TU Wien
Vienna, Austria
ender@iue.tuwien.ac.at

Simone Fiorentini
CDL for Nonvolatile Memory and Logic
Institute for Microelectronics, TU Wien
Vienna, Austria
fiorentini@iue.tuwien.ac.at

Wolfgang Goes
Silvaco Europe Ltd
Cambridge
United Kingdom
wolfgang.goes@silvaco.com

Siegfried Selberherr
Institute for Microelectronics
TU Wien
Vienna, Austria
Selberherr@TUWien.ac.at

Viktor Sverdlov
CDL for Nonvolatile Memory and Logic
Institute for Microelectronics, TU Wien
Vienna, Austria
sverdlov@iue.tuwien.ac.at

***Abstract*—We demonstrate the switching of a perpendicularly magnetized free layer by spin-orbit torques. The switching is accomplished by a purely electrical, two-current pulse scheme. The first pulse realizes the selection of the cell, while the second pulse, with a lower current, completes the switching deterministically. The second current is reduced by 50% without affecting the switching performance. This current reduction results in a reduction of about 80% of the power consumption by the second pulse. Even with such a large decrease of current and power, the switching time remains robust and fast, resulting in a very efficient switching scheme.**

***Index Terms*—Spin-orbit torque MRAM, perpendicular magnetization, magnetic field free switching, two-pulse switching scheme**

I. Introduction

The classical charge-based solid-state memory cells, the static random access memory (SRAM) cell and the dynamic random access memory (DRAM) cell, are intrinsically volatile, which has resulted in increasing standby power consumption as the cells have been downscaled. A solution to this issue can be obtained only with the introduction of nonvolatile memory cells, which must exhibit operation characteristics comparable to those of SRAM or DRAM cells [1].

Spin-transfer torque magnetoresistive random access memory (STT-MRAM) is currently the state of the art MRAM technology, with embedded STT-MRAM having densities in the order of gigabytes already demonstrated [2]. It is suitable for embedded nonvolatile memory applications as well as a replacement of flash memories [3] and L4 caches [4]. The core element of the STT-MRAM cell is a magnetic tunnel junction (MTJ), which is formed by two ferromagnetic layers separated by a tunnel barrier [5]. However, fast operation with timings in the order of nanoseconds demands large switching currents flowing through the MTJ and leading to oxide reliability issues, reducing the MRAM endurance.

Spin-orbit torque magnetoresistive random access memory (SOT-MRAM) is a promising future nonvolatile memory solution, beyond the STT-MRAM [6]. In particular, it is a viable option for a nonvolatile replacement of high-level caches, as it delivers high operation speed and large endurance. However, for a deterministic SOT switching of a perpendicularly magnetized free layer (FL) an external magnetic field is required [7], which is cumbersome for large scale integration. In order to circumvent this issue, several field-free schemes have been proposed [8], [9], [10], [11], [12].

Recently, Garello *et al.* [13] demonstrated a successful integration of a cobalt nanomagnet into the SOT cell, which provides the required magnetic field for deterministic switching. Furthermore, the approach is suitable for full 300 mm wafer fabrication [14]. In turn, Honjo *et al.* [15] showed the integration of a canted SOT cell, controlling the shape of the cell and its orientation with respect to the applied current direction, but for an in-plane magnetized FL.

An alternative, recently proposed magnetic field-free scheme is based on purely electrical switching controlled by two orthogonal current pulses. This scheme is viable for switching of both an in-plane and a perpendicularly magnetized FL [16]. Nevertheless, the large currents required to realize the switching are still an issue. They not only yield higher writing power and energy, but also make the integration of the cell in memory arrays more difficult, since they can disturb the magnetization of non-selected cells.

In this work we show that, after a pre-selection of the cell by the first current pulse, the switching current of the second pulse can be reduced by 50%, and deterministic and fast switching of a perpendicularly magnetized FL is still guaranteed. This current reduction is accompanied by a reduction of about 80% of the power consumption due to the second pulse. Even with such a large decrease of current and power, the switching time remains robust and fast, resulting in a very efficient switching scheme.

Authorized licensed use limited to: TU Wien Bibliothek. Downloaded on May 17,2021 at 07:55:35 UTC from IEEE Xplore. Restrictions apply.

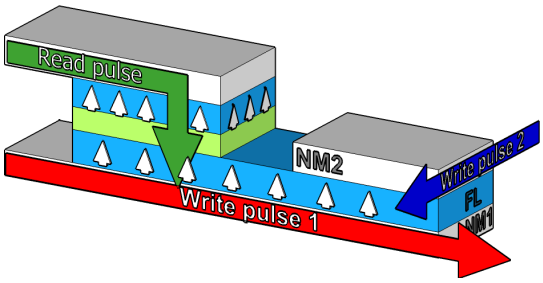

Fig. 1. SOT-MRAM cell for switching based on two orthogonal current pulses.

TABLE I
PARAMETERS USED IN THE SIMULATIONS. HEAVY METAL WIRES ARE ASSUMED TO BE β-TUNGSTEN, WHILE THE MAGNETIC FL TO BE COFEB ON MGO [7].

Parameter	Value
Saturation magnetization, M_S	1.1×10^6 A/m
Exchange constant, A	1.0×10^{-11} J/m
Perpendicular anisotropy, K	8.4×10^5 J/m^3
Gilbert damping factor, α	0.035
Spin Hall angle, θ_{SH}	0.3
Free layer dimensions	40 nm × 20 nm × 1.2 nm
NM1: $w_1 \times l$	20 nm × 3 nm
NM2: $w_2 \times l$	20 nm × 3 nm

II. SPIN-ORBIT TORQUE SWITCHING SCHEME

The memory cell is depicted in Fig. 1. The writing SOT-cell is formed by a perpendicularly magnetized FL on top of a heavy metal wire (NM1) and a second, orthogonal heavy metal wire (NM2), which contacts part of the FL. An MTJ is placed next to the SOT-cell for the reading operation.

The writing operation of the cell is carried out by applying two orthogonal current pulses. It is initiated with the selection of the cell by applying the first pulse to the NM1 wire. Physically, this pulse generates the SOT which puts the magnetization in the plane of the FL orthogonal to the current. Then, the second pulse is applied to the NM2 wire. The second pulse rotates the magnetization of the FL under the NM2 wire, which dynamically creates an in-plane magnetic field to complete the magnetization switching, and thus the cell writing, deterministically.

The reading operation is carried out by applying a low current pulse through the MTJ and sensing the corresponding tunneling magnetoresistance ratio. Since the current through the tunnel barrier of the MTJ is small, oxide reliability is not an issue.

The magnetization dynamics is described by the Landau-Lifshitz-Gilbert equation

$$\frac{\partial \mathbf{m}}{\partial t} = -\gamma\mu_0 \mathbf{m} \times \mathbf{H}_{\text{eff}} + \alpha \mathbf{m} \times \frac{\partial \mathbf{m}}{\partial t} + \frac{1}{M_S}\mathbf{T_S}, \quad (1)$$

where $\mathbf{m}$ is the normalized magnetization, γ is the gyromagnetic ratio, μ_0 is the vacuum permeability, α is the Gilbert damping factor, and M_S is the saturation magnetization. $\mathbf{H}_{\text{eff}}$ is an effective magnetic field which includes the exchange field, the uniaxial perpendicular anisotropy field, the demagnetization field, the current-induced field, and the random thermal field at 300 K. $\mathbf{T_S}$ is the SOT generated by the current, given by

$$\mathbf{T_S} = -\gamma \frac{\hbar}{2e} \frac{\theta_{SH} j}{M_S d} \left[\mathbf{m} \times (\mathbf{m} \times (\mathbf{j} \times \mathbf{z}))\right], \quad (2)$$

where e is the elementary charge, $\hbar$ is the reduced Plank constant, θ_{SH} is an effective Hall angle, j is the applied current density, d is the FL thickness, and $\mathbf{z}$ is the unit vector perpendicular to the FL plane.

To realize the SOT switching, the applied current density must be larger than the critical current density [7]

$$J_C = \frac{e}{\hbar} \frac{M_S d}{\theta_{SH}} H_K, \quad (3)$$

where H_K is the effective anisotropy field. For the two-pulse switching scheme, the selection pulse, i.e. the first pulse applied to the NM1 wire, has a current I_1 = 130 µA and a fixed duration T_1 = 130 ps. This yields a current density j_1 = 2.2×10^{12} A/m^2, which is just above the critical one (2.0×10^{12} A/m^2), given the cell parameters in Table I. In turn, the magnitude of the second current pulse (I_2), as well as the pulse duration (T_2), is varied and its impact on the switching is investigated.

The numerical simulations of the magnetization dynamics are carried out using an in-house tool [17] based on the finite differences method with a grid size of 1.2 nm. The parameters used in the simulations are listed in Table I. A stability factor of 45 is computed for the cell. In order to account for the thermal distribution resulting from the random thermal field, a total of 20 realizations are considered for each simulation condition.

III. RESULTS AND DISCUSSION

We consider, initially, a SOT-MRAM cell (Fig. 1) where the NM2 wire width (w_2) measures 20 nm. The current density of the second pulse is equal to the first pulse, i.e. I_2 = 130 µA, thus j_2 = 2.2×10^{12} A/m^2 is above the critical current density. Fig. 2 shows the z-component of the magnetization vector (average of 20 realizations) as a function of time for various pulse durations T_2. The switching is deterministic, i.e. all 20 realizations lead to magnetization switching, for all pulse durations. The switching time is practically constant at 0.3 ns (taken at m_z = -0.5) for almost all values of T_2. If the pulse duration is too short, i.e. less than 100 ps, the switching time becomes longer, as shown in Fig. 2. Nevertheless, the switching is not sensitive to small fluctuations of the pulse duration.

Since an MTJ is located beside the writing part of the SOT-cell, the NM2 wire contacts only part of the FL depending on the wire width. The switching time as a function of the NM2 wire width and of the pulse duration is shown in Fig. 3. In general the switching time increases if the pulse duration is

Authorized licensed use limited to: TU Wien Bibliothek. Downloaded on May 17,2021 at 07:55:35 UTC from IEEE Xplore. Restrictions apply.

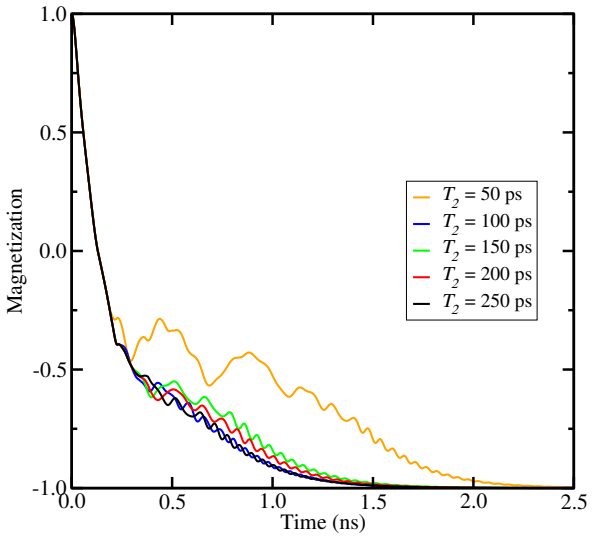

Fig. 2. z-component of the magnetization vector (average of 20 realizations) as a function of time for various pulse durations T_2. The switching is deterministic, fast, and insensitive to small pulse variations. The simulations assume $I_2 = 130\,\mu$A ($j_2 = 2.2\times10^{12}$ A/m^2).

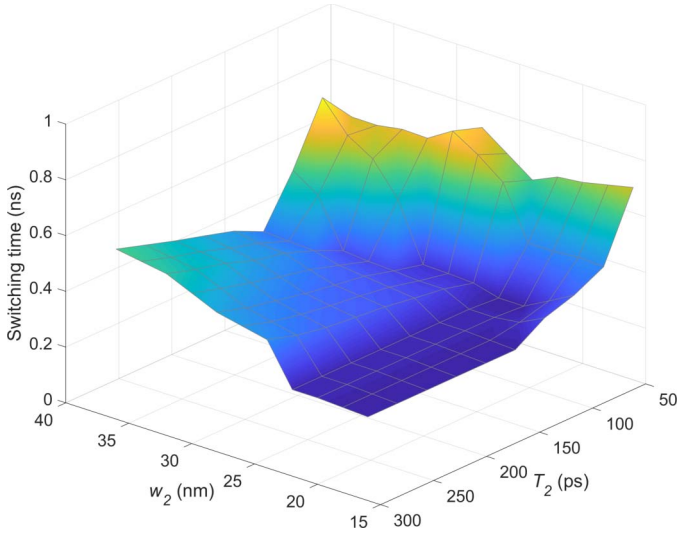

Fig. 3. Switching time as a function of the NM2 wire width and of the pulse duration. The current density $j_2 = 2.2\times10^{12}$ A/m^2 is fixed.

short, as previously observed. A similar behavior is obtained as w_2 increases, namely the switching time becomes longer the larger the NM2 wire width. Therefore, an optimal range to guarantee the fast 0.3 ns switching is found to be $16\,\text{nm} \leq w_2 \leq 24\,\text{nm}$ for the NM2 wire width and $T_2 \geq 150\,$ps for the second pulse duration. These results also indicate that, due to the relatively large range of suitable w_2 dimensions, a particularly tight control of the NM2 wire patterning is not needed.

The results shown in Fig. 3 were obtained for a constant current density, $j_2 = 2.2\times10^{12}$ A/m^2, above the critical value. Nevertheless, the current changes proportionally to w_2, i.e. $I_2 = j_2 w_2 l$. Thus, reducing the wire width leads to a

TABLE II
SECOND CURRENT MAGNITUDE AND POWER FOR DIFFERENT NM2 WIRE WIDTHS. THE CURRENT DENSITY IS FIXED AT $j_2 = 2.2\times10^{12} A/m^2$.

w_2 (nm)	I_2 (μA)	Normalized power
36	234	1.00
32	208	0.89
28	182	0.78
24	156	0.67
20	130	0.56
16	104	0.44

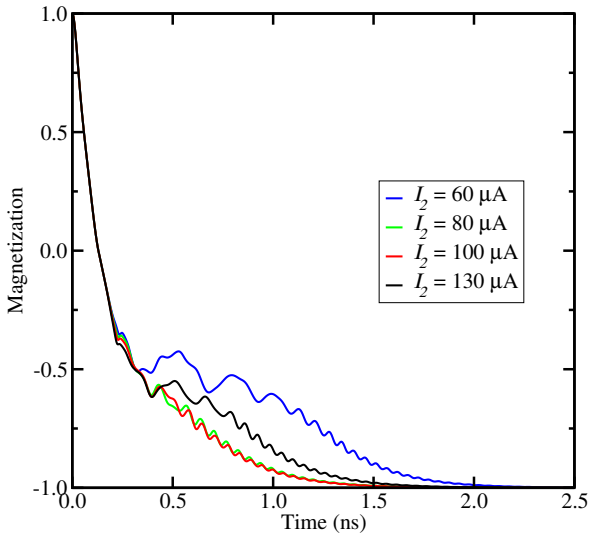

Fig. 4. z-component of the magnetization for various current pulses I_2 below the critical current and considering $w_2 = 20\,$nm. The switching is deterministic and fast even for a current 50% lower than the critical one.

reduction of the current, provided that the current density is kept constant. Lowering the current is very important and advantageous, because the switching power is also reduced, as shown in Table II.

The above approach to reduce the current is bounded by the minimum wire width. Moreover, if the NM2 wire contact with the FL becomes too narrow, the switching times increase again [16]. To further reduce the second current, and thus the power dissipation, the current density has to be decreased, pushing it below the critical value.

Fig. 4 shows the magnetization switching for several current magnitudes below the critical one, where $w_2 = 20\,$nm is fixed. Surprisingly, even for a current reduction as large as 50% in relation to the critical one ($I_c = 120\,\mu$A), the switching characteristics are still preserved, i.e. the switching remains deterministic and fast, mostly with a switching time about 0.3 ns. It was observed that the switching becomes non-deterministic for a current below 50% of the critical value.

Fig. 5 shows the switching times as a function of the second current and as a function of the pulse duration. Similar to the previous results, if the pulse becomes too short, the switching time increases rapidly. For $T_2 \geq 150\,$ps, I_2 can be decreased to 50% of the critical value without affecting the switching performance.

Authorized licensed use limited to: TU Wien Bibliothek. Downloaded on May 17,2021 at 07:55:35 UTC from IEEE Xplore. Restrictions apply.

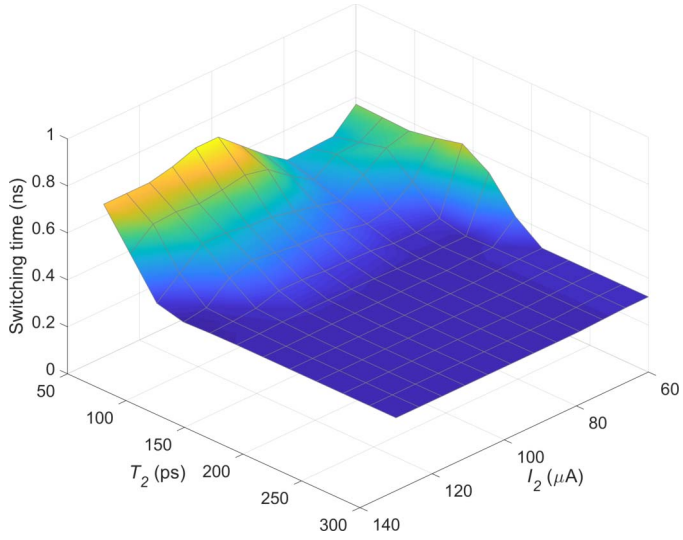

Fig. 5. Switching time as a function of the second current I_2 and as a function of the pulse duration T_2. The applied current can be significantly reduced, while the switching time remains constant.

TABLE III
CURRENT AND POWER OF THE SECOND PULSE FOR CURRENTS BELOW THE CRITICAL VALUE AND $w_2 = 20\ nm$.

I_2 (µA)	j_2 (10^{12}A/m^2)	Normalized power
130	2.2	1.00
100	1.7	0.59
80	1.3	0.38
60	1.0	0.21

As a consequence of the lower applied current, the power consumption is also significantly reduced. Table III shows the current, the current density, and the power consumption associated with the second pulse for fixed $w_2 = 20\,\text{nm}$. The power is normalized to the highest current value, taken from the previous analysis (c.f. Fig. 2). Since the power is proportional to the square of the current, a small decrease of the current results in a large reduction of the power consumption. This is clearly shown in Table III. Reducing the applied current from 130 µA to 60 µA, i.e. a reduction of 53%, the power decreases by about 80%. It should be pointed out that such a power reduction is obtained without loss in switching performance. Therefore, the efficiency of the switching scheme is significantly improved.

IV. CONCLUSION

The switching of a perpendicularly magnetized free layer by spin-orbit torques is carried out deterministically using a low current pulse. For a switching scheme based on two orthogonal current pulses, the first pulse realizes the selection of the cell, while the low current second pulse completes the switching deterministically. The switching performance remains practically unchanged even if the current is 50% lower than the critical one. In this case, we estimate a reduction of the power consumption by about 80%. Therefore, the switching becomes very efficient.

ACKNOWLEDGMENT

The financial support by the Austrian Federal Ministry for Digital and Economic Affairs and the National Foundation for Research, Technology and Development is gratefully acknowledged.

REFERENCES

[1] S.-W. Lee and K.-J. Lee, "Emerging three-terminal magnetic memory devices," *Proceedings of the IEEE*, vol. 104, no. 10, pp. 1831–1843, 2016.

[2] K. Lee, J. H. Bak, Y. J. Kim, C. K. Kim, A. Antonyan *et al.*, "1Gbit high density embedded STT-MRAM in 28nm FDSOI technology," *Proceedings of the IEDM*, pp. 2.2.1–2.2.4, 2019.

[3] O. Golonzka, J.-G. Alzate, U. Arslan, M. Bohr, P. Bai *et al.*, "MRAM as embedded non-volatile memory solution for 22FFL FinFET technology," *Proceedings of the IEDM*, pp. 18.1.1–18.1.4, 2018.

[4] J. G. Alzate, U. Arslan, P. Bai, J. Brockman, Y. J. Chen *et al.*, "2 MB array-level demonstration of STT-MRAM process and performance towards L4 cache applications," *Proceedings of the IEDM*, pp. 2.4.1–2.4.4, 2019.

[5] S. A. Wolf, D. D. Awschalom, R. A. Buhrman, J. M. Daughton, S. von Molnár *et al.*, "Spintronics: A spin-based electronics vision for the future," *Science*, vol. 294, no. 5546, pp. 1488–1495, 2001.

[6] I. M. Miron, G. Gaudin, S. Auffret, B. Rodmacq, A. Schuhl *et al.*, "Current-driven spin torque induced by the rashba effect in a ferromagnetic metal layer," *Nature Materials*, vol. 9, pp. 230–234, 2010.

[7] S. Fukami, T. Anekawa, C. Zhang, and H. Ohno, "A spin-orbit torque switching scheme with collinear magnetic easy axis and current configuration," *Nature Nanotechnology*, vol. 11, pp. 621–626, 2016.

[8] S. Fukami, C. Zhang, S. DuttaGupta, A. Kurenkov, and H. Ohno, "Magnetization switching by spin-orbit torque in an antiferromagnet-ferromagnet bilayer system," *Nature Materials*, vol. 15, pp. 535–541, 2016.

[9] Y.-W. Oh, S.-H. C. Baek, Y. M. Kim, H. Y. Lee, K.-D. Lee *et al.*, "Field-free switching of perpendicular magnetization through spin-orbit torque in antiferromagnet/ferromagnet/oxide structures," *Nature Nanotechnology*, vol. 11, pp. 878–884, 2016.

[10] H. Wu, S. A. Razavi, Q. Shao, X. Li, K. L. Wong *et al.*, "Spin-orbit torque from a ferromagnetic metal," *Physical Review B*, vol. 99, p. 184403, 2019.

[11] D. MacNeill, G. M. Stiehl, M. H. D. Guimaraes, R. A. Buhrman, J. Park, and D. C. Ralph, "Control of spin-orbit torques through crystal symmetry in WTe2/ferromagnet bilayers," *Nature Physics*, vol. 13, pp. 300–305, 2016.

[12] G. Yu, P. Upadhyaya, Y. Fan, J. G. Alzate, W. Jiang *et al.*, "Switching of perpendicular magnetization by spin-orbit torques in the absence of external magnetic fields," *Nature Nanotechnology*, vol. 9, pp. 548–554, 2014.

[13] K. Garello, F. Yasin, H. Hody, S. Couet, L. Souriau *et al.*, "Manufacturable 300mm platform solution for field-free switching SOT-MRAM," *Proceedings of the 2019 Symposium on VLSI Circuits*, pp. T194–T195, 2019.

[14] K. Garello, F. Yasin, S. Couet, L. Souriau, J. Swerts *et al.*, "SOT-MRAM 300mm integration for low power and ultrafast embedded memories," *Proceedings of the 2018 IEEE Symposium on VLSI Circuits*, pp. 81–82, 2018.

[15] H. Honjo, T. V. A. Nguyen, T. Watanabe, T. Nasuno, C. Zhang *et al.*, "First demonstration of field-free SOT-MRAM with 0.35 ns write speed and 70 thermal stability under 400°C thermal tolerance by canted SOT structure and its advanced patterning/SOT channel technology," *Proceedings of the IEDM*, pp. 28.5.1–28.5.4, 2019.

[16] V. Sverdlov, A. Makarov, and S. Selberherr, "Two-pulse sub-ns switching scheme for advanced spin-orbit torque MRAM," *Solid-State Electronics*, vol. 155, pp. 49–56, 2019.

[17] A. Makarov, "Modeling of Emerging Resistive Switching Based Memory Cells," Ph.D. dissertation, Institute for Microelectronics, TU Wien, Vienna, 2014. [Online]. Available: www.iue.tuwien.ac.at/phd/makarov/

Authorized licensed use limited to: TU Wien Bibliothek. Downloaded on May 17,2021 at 07:55:35 UTC from IEEE Xplore. Restrictions apply.